NeuroImage: Clinical 15 (2017) 710–718

Contents lists available at ScienceDirect

NeuroImage: Clinical

journal homepage: www.elsevier.com/locate/ynicl

Predicting pain relief: Use of pre-surgical trigeminal nerve diffusion metrics in trigeminal neuralgia

Peter S.-P. Hung[a,b,c], David Q. Chen[a,b], Karen D. Davis[a,b,c,d], Jidan Zhong[a], Mojgan Hodaie[a,b,c,d,*]

[a] Division of Brain, Imaging, and Behaviour - Systems Neuroscience, Krembil Research Institute, Toronto Western Hospital, University Health Network, Ontario, Canada
[b] Department of Surgery and Institute of Medical Science, Faculty of Medicine, University of Toronto, Ontario, Canada
[c] Collaborative Program in Neuroscience, University of Toronto, Ontario, Canada
[d] Division of Neurosurgery, Krembil Neuroscience Centre, Toronto Western Hospital, University Health Network, Ontario, Canada

ARTICLE INFO

Keywords:
Trigeminal neuralgia
Multi-tensor tractography
Chronic facial pain
Surgical outcome
Treatment response prediction

ABSTRACT

Trigeminal neuralgia (TN) is a chronic neuropathic facial pain disorder that commonly responds to surgery. A proportion of patients, however, do not benefit and suffer ongoing pain. There are currently no imaging tools that permit the prediction of treatment response. To address this paucity, we used diffusion tensor imaging (DTI) to determine whether pre-surgical trigeminal nerve microstructural diffusivities can prognosticate response to TN treatment.

In 31 TN patients and 16 healthy controls, multi-tensor tractography was used to extract DTI-derived metrics—axial (AD), radial (RD), mean diffusivity (MD), and fractional anisotropy (FA)—from the cisternal segment, root entry zone and pontine segment of trigeminal nerves for false discovery rate-corrected Student's *t*-tests. Ipsilateral diffusivities were bootstrap resampled to visualize group-level diffusivity thresholds of long-term response. To obtain an individual-level statistical classifier of surgical response, we conducted discriminant function analysis (DFA) with the type of surgery chosen alongside ipsilateral measurements and ipsilateral/contralateral ratios of AD and RD from all regions of interest as prediction variables.

Abnormal diffusivity in the trigeminal pontine fibers, demonstrated by increased AD, highlighted non-responders (n = 14) compared to controls. Bootstrap resampling revealed three ipsilateral diffusivity thresholds of response—pontine AD, MD, cisternal FA—separating 85% of non-responders from responders. DFA produced an 83.9% (71.0% using leave-one-out-cross-validation) accurate prognosticator of response that successfully identified 12/14 non-responders.

Our study demonstrates that pre-surgical DTI metrics can serve as a highly predictive, individualized tool to prognosticate surgical response. We further highlight abnormal pontine segment diffusivities as key features of treatment non-response and confirm the axiom that central pain does not commonly benefit from peripheral treatments.

1. Introduction

An important contemporary challenge in the surgical treatment of pain is the selection of the optimal surgical procedure that will maximize pain relief. Prediction of response will permit tailoring of treatment and facilitate individualized, patient-centered care. Classical trigeminal neuralgia (TN) is a severe chronic neuropathic facial pain disorder characterized by intermittent unilateral electric-like pain (Eller et al., 2005). TN is one of the most frequently occurring type of facial neuropathic pain (Koopman et al., 2009). While surgical treatment for TN often results in complete resolution of pain, a subgroup of patients, nonetheless, achieve minimal surgical benefit and thus require multiple, repeat interventions. TN is thought to result from neurovascular compression of the trigeminal nerve at its root entry zone (Jannetta, 1967; Love and Coakham, 2001; Nurmikko and Eldridge, 2001)—a site targeted by microvascular decompression (MVD) surgery. Less invasive procedures such as Gamma Knife radiosurgery (GKRS) instead target the cisternal segment of the trigeminal nerve by delivering of a single dose of radiation (Kondziolka et al., 1996). It is thought that TN's successful surgical outcome is partly due to its peripheral

Abbreviations: (AD), axial diffusivity; (DTI), diffusion tensor imaging; (FA), fractional anisotropy; (FSPGR), fast spoiled gradient-echo; (GKRS), Gamma Knife radiosurgery; (MD), mean diffusivity; (MR), magnetic resonance; (MVD), microvascular decompression; (RD), radial diffusivity; (ROI), region of interest; (TN), trigeminal neuralgia; (XST), eXtended Streamline Tractography

* Corresponding author at: Toronto Western Hospital, Division of Neurosurgery, 399 Bathurst Street, 4W W-443, Toronto, Ontario M5T 2S8, Canada.
E-mail address: mojgan.hodaie@uhn.ca (M. Hodaie).

http://dx.doi.org/10.1016/j.nicl.2017.06.017
Received 12 January 2017; Received in revised form 26 May 2017; Accepted 10 June 2017
Available online 12 June 2017

pathophysiology. In contrast, other forms of neuropathic pain tend to not respond as well to treatment. For those patients, neuromodulation strategies such as deep brain stimulation can be relied upon (Boccard et al., 2013; Hodaie and Coello, 2013). While many TN patients achieve pain relief after their first surgical procedure for TN, nearly 20% of patients either do not respond or have very early recurrence of TN pain within a year and thus require additional surgeries for TN (Dhople et al., 2009; Hodaie and Coello, 2013; Oesman et al., 2011). It is currently unclear what distinguishes these two populations apart from each other. Pre-surgical differentiation of these groups, in particular, the prediction of non-response may allow clinicians to optimize surgical treatment of TN patients—minimizing unnecessary procedures.

Diffusion tensor imaging (DTI) is a non-invasive magnetic resonance (MR) imaging technique that allows *in vivo* visualization of white matter tracts (Alexander et al., 2007). Specific diffusion metrics—axial (AD), radial (RD) and mean diffusivities (MD), as well as a composite metric, fractional anisotropy (FA)—can provide scalar measures of white matter microstructural properties. Biologically, AD, RD, MD have been linked with axonal integrity (Brennan et al., 2013; Song et al., 2003), degree of myelination (Brennan et al., 2013; Song et al., 2005, 2003), and underlying neuro-edema (Beaulieu, 2002), respectively. Similarly, FA provides insight into white matter integrity and has been shown to be altered in various human diseases associated with chronic pain such as temporomandibular disorder (Moayedi et al., 2012) and multiple sclerosis (Chen et al., 2015). Current DTI analyses are limited to the periphery due to crossing nerve fibers in the brainstem and demonstrate that patients with TN have lower FA and higher AD, RD, and MD within the TN-affected, ipsilateral trigeminal nerve root entry zone (DeSouza et al., 2014; Herweh et al., 2007; Leal et al., 2011). With eXtended Streamline Tractography (XST) (Qazi et al., 2009)—a multi-tensor deterministic DTI tractography algorithm—our group recently overcame this technical limitation and successfully visualized brainstem trigeminal fibers (Chen et al., 2015). Thus, using XST DTI, here we aim to investigate both peripheral and brainstem portions of the trigeminal nerve and to identify pre-surgical diffusivity patterns that distinguishes long-term responders from non-responders. We hypothesize that there are pre-surgical trigeminal nerve microstructural differences between long-term responders and non-responders–possibly due to a more severe and central TN pathology affecting non-responders.

2. Material and methods

2.1. Research subjects

With University Health Network Research Ethics Board approval, a total of 31 patients with classic, type 1 TN characterized by recurrent episodes of severe, lancinating, electric shock-like pain (Eller et al., 2005) were identified through retrospective chart reviews spanning from 2011 to 2015. Only patients without prior surgical treatment for TN were included in this study. Patients with TN secondary to multiple sclerosis, cranial tumors, or vertebrobasilar dolichoectasia resulting in brainstem compression were excluded from this study. Based on an all-or-none presence of TN pain at least one year after their first surgical treatment for TN (GKRS or MVD), we subdivided these patients into 17 long-term responders and 14 non-responders to neurosurgical therapy of TN (Table 1). At this time point, patients with any TN pain were deemed non-responders while those without pain were responders. 16 healthy control subjects were also recruited. Ipsilateral and contralateral nerves in these controls were based on the laterality of TN in matched patients. That is, controls matched to left TN patients will have ipsilateral nerve on the left, and vice versa. Research ethics approval was obtained for both retrospective chart review and MR imaging—including DTI—of patients with TN. Similarly, recruitment and MR imaging of healthy controls was conducted with institutional research ethics board approval. The images of six TN patients were reported as part of a prior study (DeSouza et al., 2014).

Table 1
Trigeminal neuralgia patient demographics.

ID	Group	Sex	Age	TN side	Affected branches	Surgical treatment	Pain med(s)
P01	Responder	F	70	L	V2/3	GKRS	PGB
P02	Responder	F	65	L	V3	GKRS	GPN
P03	Responder	F	71	L	V2/3	GKRS	None
P04	Responder	M	36	L	V2	MVD	CBZ
P05	Responder	M	44	R	V2/3	MVD	CBZ
P06	Responder	M	53	R	V1	MVD	CBZ
P07	Responder	F	79	R	V3	GKRS	CBZ
P08	Responder	F	65	R	V2	GKRS	CBZ, GPN
P09	Responder	M	59	R	V1/2	GKRS	CBZ
P10	Responder	F	76	R	V2/3	GKRS	CBZ
P11	Responder	F	77	R	V2/3	GKRS	GPN
P12	Responder	F	56	L	V1/2	MVD	GPN
P13	Responder	F	75	R	V2/3	GKRS	GPN
P14	Responder	F	59	R	V1/2/3	GKRS	PGB, CBZ
P15	Responder	F	47	R	V1/2/3	GKRS	GBP, CBZ
P16	Responder	M	38	R	V2	GKRS	CBZ, PGB
P17	Responder	F	52	R	V1	MVD	CBZ
P18	Non-responder	F	54	L	V1/2/3	MVD	CBZ
P19	Non-responder	F	43	L	V1/2/3	MVD	GBP
P20	Non-responder	F	78	R	V2/3	GKRS	OCZ
P21	Non-responder	F	50	L	V2	GKRS	CBZ
P22	Non-responder	F	63	L	V1/2	MVD	CBZ
P23	Non-responder	F	38	R	V1/2	GKRS	GPN
P24	Non-responder	M	66	R	V2/3	MVD	CBZ, PGB
P25	Non-responder	F	47	R	V1/2/3	GKRS	CBZ, PGB
P26	Non-responder	M	64	R	V3	GKRS	None
P27	Non-responder	F	46	R	V3	GKRS	PGB
P28	Non-responder	F	70	R	V2	GKRS	CBZ
P29	Non-responder	M	25	R	V3	MVD	CBZ
P30	Non-responder	M	62	R	V1/2/3	GKRS	PGB
P31	Non-responder	F	73	R	V2/3	GKRS	GPN

Abbreviations: PGB = pregabalin, GPN = gabapentin, CBZ = carbamazepine, OCZ = oxcarbazepine.

2.2. Magnetic resonance image acquisition

For all subjects, pre-surgical high resolution, T1 fast spoiled gradient-echo (FSPGR) anatomical and diffusion-weighted whole-head MR images were acquired on a 3 Tesla GE Signa HDx scanner with an 8 channel head coil. The FSPGR MR image acquisition parameters were: voxel size = 0.94 mm × 0.94 mm × 1 mm, 256 × 256 matrix, *TE* = 5.1 ms, *TR* = 12.0 ms, flip angle = 20°, field of view = 24 cm (controls) and 22 cm (patients). The diffusion-weighted MR image acquisition parameters were: 60 directions, 1 B_0, b = 1000 s/mm^2, spin echo EPI sequence, 1 excitation, ASSET, voxel size = 0.94 mm × 0.94 mm × 3 mm, 128 × 128 matrix, *TE* = 86.4 ms, *TR* = 17 s (controls) and 12 s (patients), flip angle = 90°, field of view = 24 cm.

2.3. Magnetic resonance image processing

Eddy current and motion artifacts within diffusion-weighted MR images were corrected with affine transformations of each subject's gradient images to B_0 image in FSL v 5.0 (Smith et al., 2004). In order to estimate subject-specific diffusion tensor images and scalar diffusion metric images (i.e. FA, AD, RD, and MD), diffusion-weighted MR images were further processed in 3D Slicer v 4.3.1 (Fedorov et al., 2012). Trigeminal nerves for each subject were then virtually reconstructed bilaterally from diffusion-weighted MR images using XST (Westin planar cut-off = 0.2, tensor fraction cut-off = 0.2, minimum

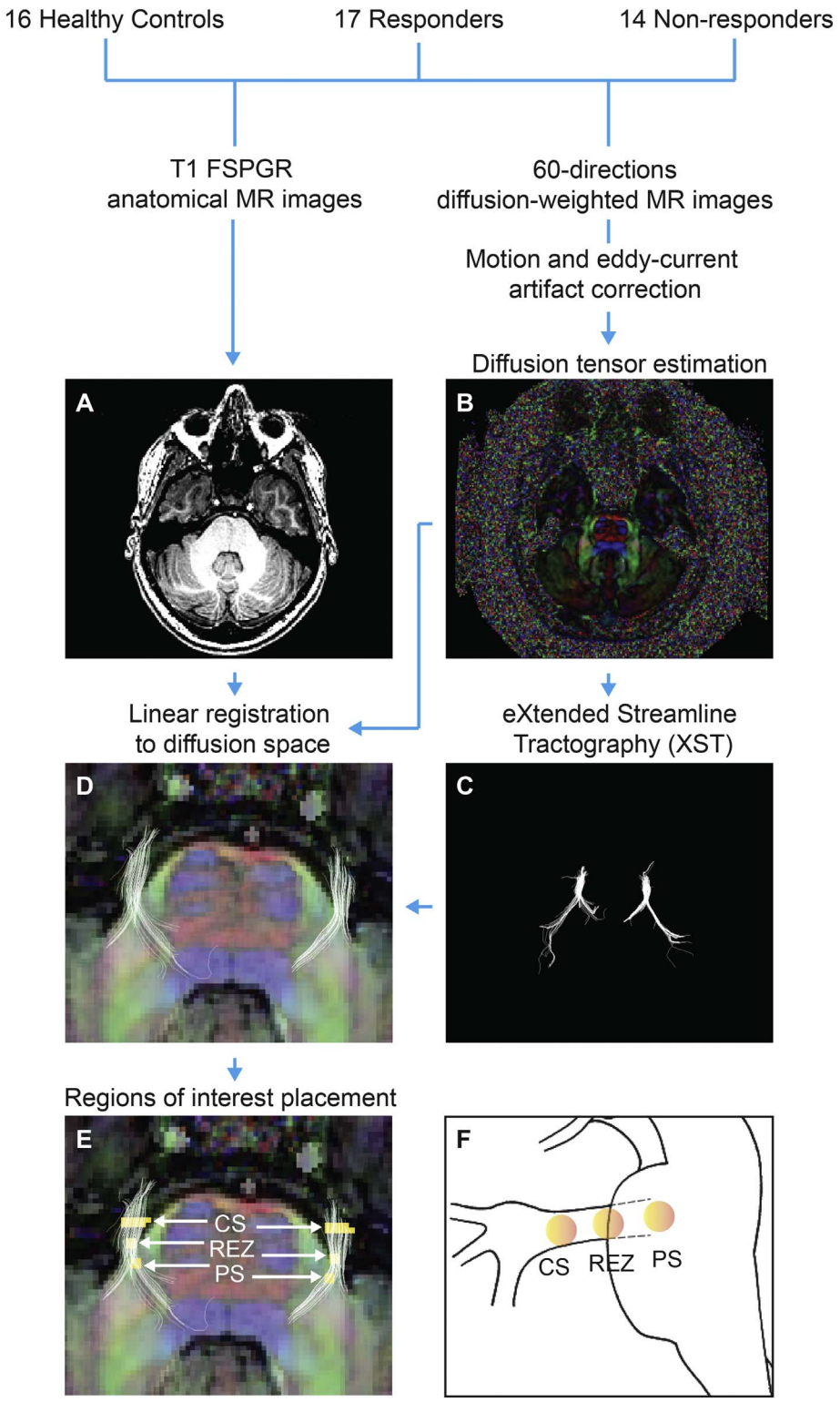

Fig. 1. Magnetic resonance image processing pipeline. For all study participants, T1 anatomical (A) and 60 directions diffusion-weighted MR images were acquired on a 3 Tesla MR scanner. Diffusion-weighted MR image was first corrected for motion and eddy current acquisition artifacts; after which, it was used to construct diffusion tensor image (B) and bilateral trigeminal nerves (C) via XST algorithm. T1 anatomical MR image (A) was linearly aligned to diffusion tensor image (B) and overlaid with bilateral XST-reconstructed trigeminal nerves (C). Panel D demonstrates the result of this process for a single subject in axial color-by-orientation view (red: left-right, green: anterior-posterior, blue: superior-inferior). Once image processing was complete, regions of interest (E, yellow) were placed bilaterally at mid-pontine level of the brainstem in diffusion space at the cisternal segment (CS), root entry zone (REZ), and pontine segment (PS) along XST-generated trigeminal nerves. Shown in F is a sagittal brainstem view of these regions of interests.

radius of curvature = 0.8 mm, minimum length = 10 mm, step size = 1 mm, seeded from 1 mm coronal cross section of trigeminal nerve). T1 FSPGR anatomical MR images were linearly aligned to diffusion space—emphasizing fine alignment of the mid-pontine region where trigeminal nerves enter the brainstem. Both XST-reconstructed nerves and aligned T1 image guided bilateral region of interest (ROI) definition within each subject at the trigeminal nerve cisternal segment, root entry zone, and pontine segment. Fig. 1 provides a schematic of this MR image processing pipeline.

2.4. Experimental design

During ROI placement, the experimenter was blinded as to whether the participant belonged to the healthy control, responder, or non-responder group. Subject images were coded with an anonymization program written in Python. Decoding of subject group membership only occurred after ROI definition was completed for all subjects. Three ROIs were delineated bilaterally in each study participant at the trigeminal nerve cisternal segment, root entry zone, and the pontine segment

(Fig. 1E). The trigeminal cisternal segment ROI consisted of 2 coronal planes (20–22 voxels in total) transecting XST-reconstructed trigeminal nerves half way between the trigeminal ganglion and root entry zone (Chen et al., 2015). The trigeminal root entry zone ROI was four voxels in size, oriented in an axial plane, with two voxels each from the trigeminal cisternal segment and pontine segment (DeSouza et al., 2015, 2014). The trigeminal pontine segment ROI was identical in size to the root entry zone ROI and was positioned at least two voxels further along XST-reconstructed nerves towards the brainstem than root entry zone ROI. From all ROIs, microstructural diffusivity metrics (FA, AD, RD, and MD) were extracted in 3D Slicer.

2.5. Statistical analyses

For each ROI, we used six hypothesis-driven two-tailed Student's *t*-tests to test for differences between pre-surgical microstructural diffusivities from TN-affected and contralateral trigeminal nerves in long-term responders, non-responders, and healthy controls. Within-group comparisons of ipsilateral versus contralateral trigeminal nerves were computed as paired *t*-tests while between-group comparisons of ipsilateral trigeminal nerves were computed as independent *t*-tests. Multiple comparisons were statistically corrected with the false discovery rate procedure (Benjamini and Hochberg, 1995). Average diffusivity metrics for each group at each ROI were bootstrap resampled to n = 2000 level to visualize possible pre-surgical thresholds of response to surgical treatment for TN. Bootstrap resampling here involved randomly picking 3 out of 31 measurements with replacement over 2000 iterations, obtaining the mean for each iteration, and sorting the means in ascending order to facilitate confidence interval calculation. In order to construct a statistical classification model predictive of long-term surgical response, ipsilateral/contralateral diffusivity ratios and raw ipsilateral measurements of AD and RD at cisternal segment, root entry zone, and pontine segment alongside the type of surgery chosen were then submitted to a discriminant function analysis. Only AD and RD from each ROI were included in the model as they are mathematically distinct from each other, since they are calculated using distinct eigenvalues (Mukherjee et al., 2008). Statistical significance was set at $p < 0.05$ and all analyses were computed using R Statistics Software Suite v 3.23 (Ross et al., 1996). DFA model was also assessed with leave-one-out-cross-validation (LOOCV) and Chi-square test of association between predicted and true response groups.

3. Results

3.1. Experimental groups

This study consisted of three subject groups: 17 responders (12 females, 36–79 years, 60.1 ± 13.7 years s.d.), 14 non-responders (10 females, 25–78 years, 55.6 ± 14.9 years s.d.), and 16 healthy controls (eight females, 25–66 years, 49.3 ± 11.7 years s.d.). Average age at the time of MR image acquisition were not statistically different across long-term responders, non-responders and healthy controls ($F_{(2)} = 2.67$, $p = 0.08$). The proportion of sex in each group was also not significantly different ($\chi^2_{(2)} = 2.01$, $p = 0.37$). Furthermore, the ratio of the type of surgery chosen in each patient group was statistically non-significant ($\chi^2_{(1)} = 0.14$, $p = 0.71$).

3.2. TN-induced cisternal segment microstructural alterations in long-term responders

Pre-treatment DTI metrics of the long-term responders showed significantly lower MD ($t_{(16)} = -3.15$, $p = 0.037$) and AD ($t_{(16)} = -3.21$, $p = 0.033$) within the cisternal segment of TN-affected trigeminal nerve compared to contralateral asymptomatic nerve (Fig. 2A). At the trigeminal root entry zone (Fig. 2B), both long-term responders and non-responders had significantly higher ipsilateral trigeminal nerve AD, RD, and MD compared to contralateral nerves and healthy controls (corresponding t-statistics shown in Table 2). At the pontine segment (Fig. 2C), ipsilateral and contralateral nerves in long-term responders were not statistically different from those of healthy controls.

Table 2
Student's t-statistics for microstructural diffusivities at the root entry zone.

	Diffusivity	t-Value	Degrees of freedom	FDR p-value	Significance
Responders: Ipsilateral compared to contralateral nerves	AD	3.4	16	0.022	*
	RD	3.21	16	0.016	*
	MD	3.37	16	0.016	*
	FA	−2.54	16	0.043	*
Non-responders: Ipsilateral compared to contralateral nerves	AD	2.47	13	0.043	*
	RD	2.94	13	0.017	*
	MD	2.79	13	0.023	*
	FA	−3.44	13	0.026	*
Responders: Ipsilateral compared to healthy controls	AD	2.54	29.3	0.033	*
	RD	2.75	24.51	0.017	*
	MD	2.72	26.29	0.023	*
	FA	−1.94	31	0.093	n.s.
Non-responders: Ipsilateral compared to healthy controls	AD	2.66	26.08	0.033	*
	RD	3.17	19.85	0.016	*
	MD	3.09	22.36	0.016	*
	FA	−2.45	25.32	0.043	*

Abbreviations: FDR p-value = false discovery rate-adjusted p-value, n.s. = not significant.
* $p < 0.05$.

3.3. TN-related root entry zone and pontine segment microstructural alterations in non-responders

Non-responders had significantly lower FA at the root entry zone of ipsilateral TN-affected nerve compared to matched healthy control nerves ($t_{(25.323)} = -2.45$, $p = 0.043$) (Fig. 2B). In addition, a significantly higher AD ($t_{(14.474)} = 3.24$, $p = 0.034$) was observed in the pontine segment of ipsilateral TN-affected trigeminal nerve of non-responders compared to matched healthy controls (Fig. 2C). Within the trigeminal nerve cisternal segment, both ipsilateral TN-affected and contralateral asymptomatic nerves in non-responders were not statistically different from healthy controls (Fig. 2A).

3.4. Bootstrap resampling of DTI metrics revealed ipsilateral diffusivity thresholds of surgical response

There were three ipsilateral diffusivity thresholds of response to treatment obtained from the bootstrap resampled 85% confidence intervals of AD, RD, MD, and FA along bilateral trigeminal nerves in long-term responders and non-responders. We defined these diffusivity thresholds of response as cut-off points at which ≤ 50% of responders and ≥ 85% of non-responders were observed (Fig. 3, black bars). TN patients with diffusion metrics above (in the case of AD and MD) or below (in the case of FA) of these thresholds along ipsilateral trigeminal nerve were less likely to respond to their surgical treatment. Of the three unique diffusivity thresholds, two were localized to the pontine segment of the trigeminal nerve (AD and MD, Fig. 3A) while one was in cisternal segment of the nerve (FA; Fig. 3B).

3.5. Discriminant function analysis produced a highly predictive statistical prognosticator of response

Discriminant function analysis of ipsilateral/contralateral ratios and ipsilateral measurements of AD and RD across all three regions of interest alongside the type of surgery chosen produced a highly accurate statistical classifier (Table 3). Using pre-surgical diffusivities, this

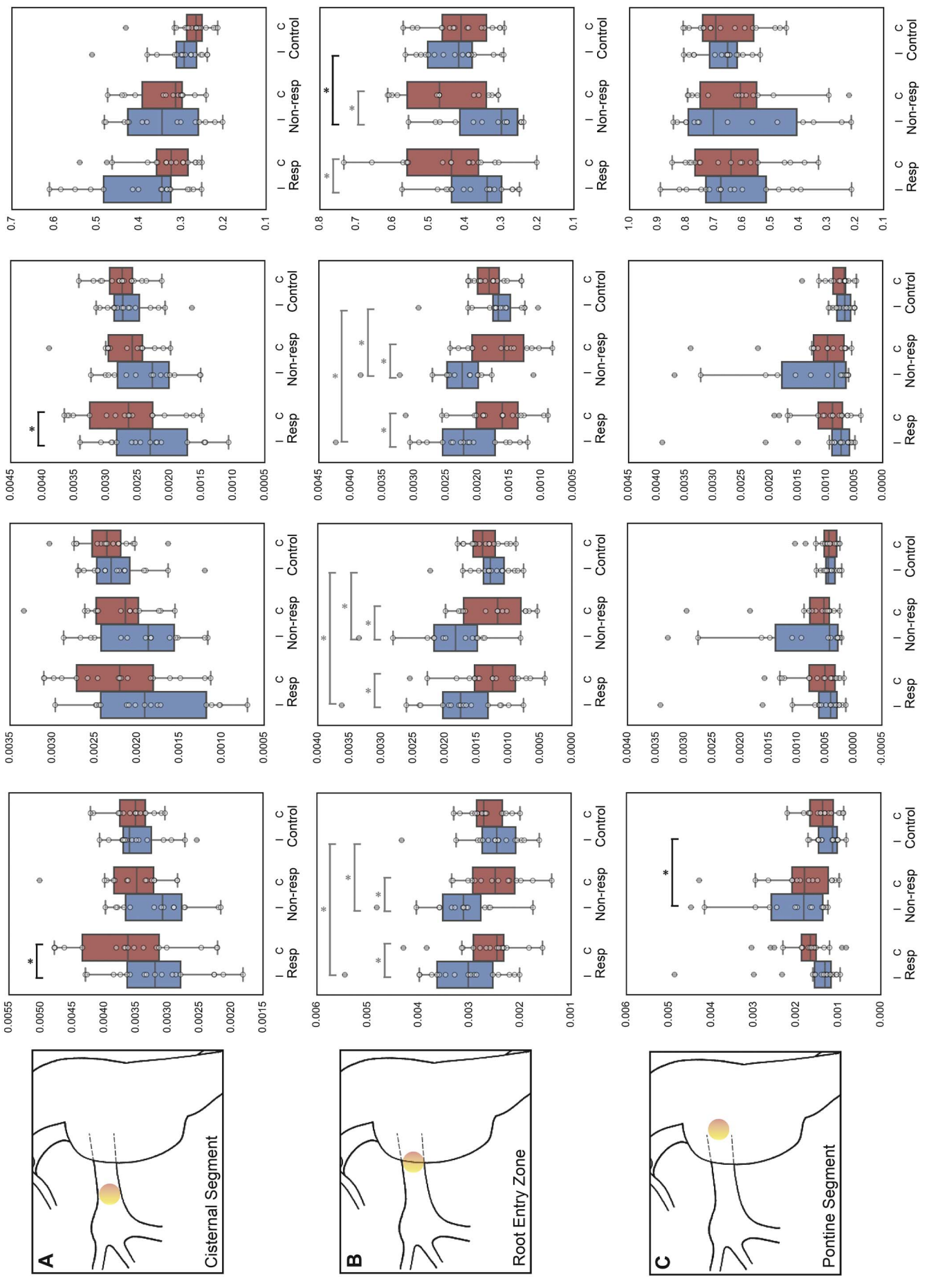
Axial Diffusivity
Radial Diffusivity
Mean Diffusivity
Fractional Anisotropy
I_C Resp
I_C Non-resp
I_C Control
A
Cisternal Segment
B
Root Entry Zone
C
Pontine Segment

Fig. 2. Microstructural diffusivities along trigeminal nerves reveal abnormalities distinguishing response groups.
Diffusion tensor imaging-derived metrics (AD, RD, MD and FA) were extracted from ipsilateral and contralateral trigeminal nerves in responders, non-responders, and healthy controls (black whiskers denote 1.5 interquartile ranges, horizontal lines within boxes indicate group medians and circles are individual subject measurements). False discovery rate-adjusted Student's *t*-tests revealed uniquely lower ipsilateral versus contralateral nerve AD and MD in the cisternal segment (row A) in responders. Non-responders, on the other hand, had characteristically lower FA in the ipsilateral nerve root entry zone (row B) and higher ipsilateral AD in the pontine segment (row C) of the nerve compared to healthy controls. Black braces indicate characteristic microstructural diffusivity changes while grey braces are shared changes between responders and non-responders.
Abbreviations: Resp = responder, Non-resp = non-responder, I = ipsilateral, C = contralateral, * = $p < 0.05$.

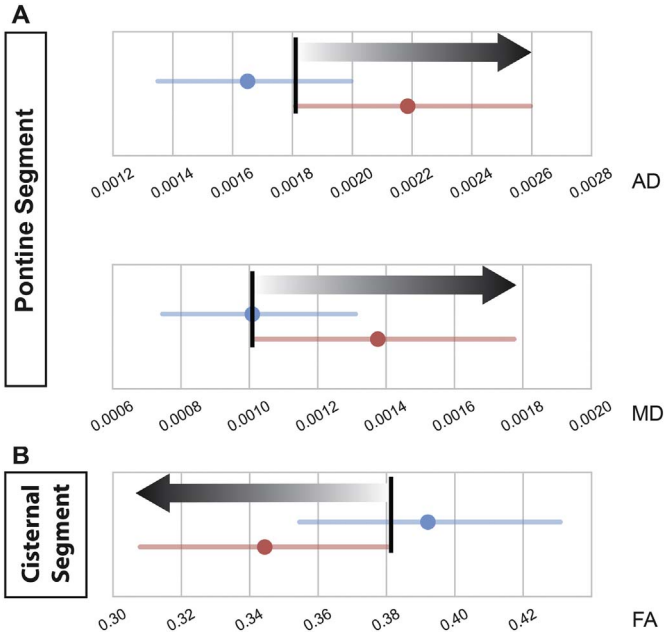

Fig. 3. Differences in bootstrap resampled microstructural diffusivities in symptomatic trigeminal nerve define likelihood of non-response after surgical treatment of TN.
Comparisons of bootstrapped (n = 2000) 85% confidence intervals of symptomatic nerve microstructural diffusivities of long-term responders (blue) and non-responders (red) to surgical treatment for TN at the pontine segment (A) and cisternal segment (B) revealed three thresholds of response at which ≤ 50% long-term responders and ≥ 85% non-responders were observed (threshold = vertical black bar). Grey gradient arrows indicate increasing likelihood of non-responsiveness to surgery.
Abbreviations: AD = axial diffusivity, RD = radial diffusivity, MD = mean diffusivity, FA = fractional anisotropy.

Table 3
Discriminant function analysis coefficients ranked by absolute magnitude.

Predictor	Absolute coefficient of discriminant function	z-Score	% contribution to linear discriminant function
Ipsilateral PS RD	12,912.25	− 2.064	27.438
Ipsilateral PS AD	11,366.43	1.784	24.153
Ipsilateral CS RD	10,920.01	1.714	23.204
Ipsilateral CS AD	7170.414	− 1.154	15.237
Ipsilateral REZ AD	2724.719	− 0.449	5.79
Ipsilateral REZ RD	1940.773	0.29	4.124
I/C ratio of CS AD	9.257	− 0.016	0.02
I/C ratio of CS RD	8.299	− 0.019	0.018
Surgical treatment modality	3.445	− 0.018	0.007
I/C ratio of PS AD	2.768	− 0.017	0.006
I/C ratio of REZ RD	0.936	− 0.017	0.002
I/C ratio of REZ AD	0.825	− 0.017	0.002
I/C ratio of PS RD	0.301	− 0.017	0.001

Abbreviations: I/C ratio = ipsilateral/contralateral diffusivity ratio, REZ = root entry zone, PS = pontine segment, CS = cisternal segment.

prognosticator correctly classified 26 of the 31 TN patients—82.4% (14 out of 17) responders and 85.7% (12 out of 14) non-responders—to their respective groups. Absolute coefficients of linear discriminants from this prognosticator (Table 3) revealed that ipsilateral pontine segment AD and RD are the two best predictors of long-term surgical response which together account for 51.6% of the classifier's prognostication success. The approximate out-of-group testing accuracy of our DFA model using LOOCV was 71.0%. A Chi-square test yielded a significant association between predicted and true response groups ($\chi^2_{(1)} = 6.419$, $p = 0.011$).

4. Discussion

We demonstrate for the first time that pre-treatment diffusivities along symptomatic trigeminal nerves can prognosticate surgical outcome in classical TN, and accurately differentiate responders from non-responders. Of the various DTI metrics and anatomical sites studied, the key site that distinguished non-responders was the pontine segment. The pontine segment had not been previously implicated as having a role in the pathophysiology of TN, and could only be studied recently using the novel method of multi-tensor deterministic tractography—-given the large number of crossing fibers in this region (Chen et al., 2015; Qazi et al., 2009). This finding suggests that more central TN-induced changes are responsible for lack of treatment response, and point to a dynamic process whereby a peripheral insult (neurovascular compression) can potentially result in eventual central microstructural changes, a finding not demonstrated before using *in vivo* imaging techniques. Altogether three unique, pre-treatment diffusivity thresholds of response were identified through bootstrap re-sampling—allowing us to distinguish 85% of non-responders from responders. Discriminant function analysis of pre-treatment ipsilateral/contralateral ratio and ipsilateral measurements of axial and radial diffusivities alongside the type of surgery chosen further permitted the construction of a highly successful (83.9% accurate) prognostication tool of surgical response. This is of important value in our goal of developing *in vivo*, personalized paradigms of surgical care for TN.

4.1. DTI reveals novel trigeminal nerve microstructural patterns of response to surgical treatment for TN

While conceptually the root entry zone could be thought of as the most relevant site of diffusivity metrics abnormalities in TN, we found this site to be a relatively minor contributor to the distinction between responders and non-responders. This is because the root entry zone demonstrates differences across all TN patients–responders and non-responders and therefore does not serve as a strong prognosticator (Fig. 2B). The importance of the root entry zone diffusivity abnormalities in TN has been demonstrated previously by others as well as our own previous reports (DeSouza et al., 2014; Herweh et al., 2007; Leal et al., 2011). We did, however, observe that the magnitude of difference in DTI metrics in the root entry zone differed between responders and non-responders, suggesting that there are more pronounced abnormalities that characterize non-responders (Fig. 2B). Therefore, larger magnitude of diffusivity alterations along a TN-affected nerve may be associated with greater likelihood for a treatment non-response, and possibly, the severity of neurovascular compression or other neuronal abnormalities.

Major distinctions between responders and non-responders appear to lie in diffusivity alterations elsewhere along the trigeminal system. In particular, non-responders demonstrated a characteristically higher AD at the pontine segment (Fig. 2C). Given that AD changes are presumed to be associated with axonal changes (Song et al., 2002, 2003), this suggests that non-responders may have axonal abnormalities. This is unlike the pattern of diffusivity abnormalities in patients with TN secondary to multiple sclerosis which includes RD and MD abnormalities (Chen et al., 2015)—demonstrating possible altered myelination (Song et al., 2005) and underlying neuro-inflammation (Beaulieu, 2002), respectively. Long-term responders, on the other hand, showed lower MD and AD at the cisternal segment—suggesting possible underlying neuro-inflammation and axonal alterations (Fig. 2A). Given that MVD and GKRS do not address more central components of the trigeminal system (at the pontine segment of the nerve) these procedures cannot ameliorate the TN-induced microstructural changes in non-responders and thus reasonably contribute to poor surgical treatment outcomes.

4.2. DTI uncovers group-level microstructural diffusivity thresholds of response to surgical treatment of TN

All 12 possible combinations of microstructural diffusivities (AD, RD, MD, and FA) across ROIs (cisternal segment, root entry zone, and pontine segment) were bootstrap resampled to construct 85% confidence intervals for responders and non-responders. This allowed us to, at a group-level, identify three ipsilateral trigeminal nerve diffusivity thresholds of response which separated ≥ 85% of non-responders from responders to TN treatment. Two out of three of these thresholds were located in the pontine segment, with pontine segment AD providing the best separation between response groups (Fig. 3). While these findings further highlight the importance of pontine segment diffusivities as differentiators of treatment response, from a fundamental perspective, they also point to the need to increase our understanding of what occurs at the level of the nerve to result in significant alterations in diffusivities. Whether any such changes correlate with degree of compression/distortion of the nerve, duration of symptoms, or potentially other neuronal changes remains to be examined (Love and Coakham, 2001; Maarbjerg et al., 2015).

4.3. Pre-surgical ipsilateral pontine segment AD and RD are highly predictive of individual surgical response

Group-level pre-surgical diffusivity thresholds of response obtained from bootstrap resampling do not allow prediction of individual response. As such, in order to transform group-level predictors of surgical response identified above into a practical individual-level prognostication solution, we further conducted a discriminant function analysis involving the type of surgery chosen and the ipsilateral/contralateral diffusivity ratios alongside ipsilateral measurements of AD and RD across all three regions of interests of the trigeminal nerve. Mathematically, the equations for the DTI metrics are as followed (Mukherjee et al., 2008):

$$AD = \lambda 1$$

$$RD = \frac{(\lambda 2 + \lambda 3)}{2}$$

$$MD = \frac{(\lambda 1 + \lambda 2 + \lambda 3)}{3}$$

$$FA = \sqrt{\frac{3((\lambda 1 - MD)^2 + (\lambda 2 - MD)^2 + (\lambda 3 - MD)^2)}{2(\lambda 1^2 + \lambda 2^2 + \lambda 3^2)}}$$

As such, AD and RD were consciously chosen over MD and FA for the discriminant function analysis to ensure that each unique eigenvalue (λ1, λ2, λ3) associated with the diffusion tensor was represented only once in resulting statistical model. Ratios of ipsilateral/contralateral AD and RD were also included in the model in order to reflect within-subject deviation in trigeminal nerve microstructure from asymptomatic contralateral levels.

Discriminant function analysis produced a highly predictive (83.9% accurate) statistical classifier of treatment response for surgically naïve TN patients. Absolute coefficient of discriminant function (Table 3) indicated that ipsilateral diffusivities are superior than ipsilateral/contralateral ratios of diffusivities as predictors of surgical response. Furthermore, ipsilateral pontine segment diffusivities contributed significantly more so than cisternal segment and root entry zone diffusivities to this classifier's prediction success—contributing 51.6% versus 38.4% and 9.9%, respectively (Table 3). As such, in order to predict treatment success in TN patients, it may be important to include comprehensive pre-surgical DTI assessment of trigeminal nerves—especially more central portions of the nerve—in routine imaging of TN patients. Pathophysiologic factors leading to microstructural abnormalities involving these portions of the trigeminal system in non-responders warrant further studies. Unlike TN secondary to multiple

sclerosis, little is known of the more central portions of this system in classic TN (Chen et al., 2015). In order to construct a clinical composite of TN patients, future studies are needed to examine how individual variability in DTI measures along central and peripheral portions of symptomatic trigeminal nerves are related to the clinical presentation of TN (i.e. degree of neurovascular contact, coverage of trigeminal dermatomes, and more).

To date there are no imaging markers, patterns, or tools that can distinguish TN surgical responders from non-responders. In light of the highly successful statistical classifier of surgical response we constructed in this study from novel pre-surgical trigeminal nerve microstructure patterns and thresholds of treatment response, we foresee the integration of microstructural integrity assessments of trigeminal nerves into the selection process of neurosurgical treatments for TN.

4.4. Study limitations

Our study utilized bootstrap resampling to obtain ipsilateral diffusivity thresholds of response to surgeries for TN. Bootstrap resampled distributions cannot exceed the range of the initial data (diffusivities) distribution. As such, in order to obtain bootstrap resampled distributions that most closely resemble the true population distribution, it is important to maximize the sample size of the initial data. In this study, we had diffusivity metrics from 17 responders and 14 non-responders—which may have been somewhat limited. As such, additional patients are being recruited to allow us to improve our bootstrap approximation of ground-truth distribution for each response group and validate our three group-level thresholds of response.

Through discriminant function analysis of ipsilateral/contralateral ratios, ipsilateral measurements of AD and RD, and the type of surgery we were able to create a highly successful classifier of surgical response. One important caveat here is that our success rate of 83.9% was obtained by testing the classifier against its own training group. Through a leave-one-out-cross-validation—which is well-suited for studies with smaller sample sizes—we were able to determine that our classifier has an approximate testing accuracy of 71.0%. Further prospective testing is important for us to ascertain if this approximation holds true. As such, once we have amassed an appropriate cohort of TN patients, we plan to do so.

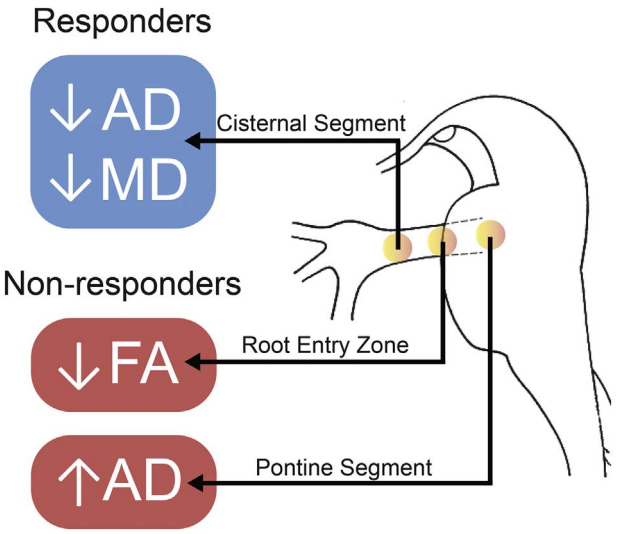

Fig. 4. Unique patterns of pre-surgical diffusivity alterations distinguish responders from non-responders.
Key pre-surgical DTI metric patterns differentiating long-term responders from non-responders along symptomatic trigeminal nerves are shown. Long-term responders (in blue) have unique microstructural abnormalities localized to the trigeminal nerve cisternal segment (CS) whereas non-responders (in red) have abnormalities located more centrally—at the root entry zone (REZ) and pontine segment (PS) of the nerve. The illustration on the right is a sagittal view of the brainstem. Yellow-orange dots in this view illustrate these key regions of interest from which DTI metrics were gathered.

5. Conclusions

We have detailed novel pre-surgical microstructural abnormalities in the peripheral and central nervous system in classical TN patients that permit us to predict long-term pain relief after TN surgical treatment (Fig. 4). Our study highlights the important role of DTI-derived metrics in the study of *in vivo* abnormalities of chronic pain and adds to our knowledge the unique finding of pontine changes in non-responders—suggesting a dynamic nature of peripheral and central changes in neuropathic pain. Current literature shows that TN also induces grey and white matter abnormalities in CNS areas important for sensory and cognitive-affective dimensions of pain (Desouza et al., 2013; DeSouza et al., 2014). It is thus possible that these TN-induced structural alterations can have functional consequences—resulting central manifestations of TN pain. As such, future imaging studies should be multimodal in nature—utilizing anatomical, diffusion, and functional MR imaging—in order to ascertain if this is indeed the case and identify potential pre-surgical functional prognosticators of response to TN surgery.

Acknowledgements

The authors would like to thank Tessa Burkholder and Erika Wharton-Shukster for their assistance with chart reviews, and Kevin E. Liang for MR image retrieval and maintenance of the healthy control database.

This study is supported by Canadian Institutes of Health Research operating grant (Ref. # MOP130555), the Trigeminal Neuralgia Association of Canada, and the Ontario Graduate Scholarship program. MH has received previous research grants from Elekta. MH holds active grants from the Canadian Institutes of Health Research and the Multiple Sclerosis Society of Canada. KDD is supported by a Mayday fund grant. Otherwise, the authors report no conflicts of interest.

References

Alexander, A.L., Lee, J.E., Lazar, M., Field, A.S., 2007. Diffusion tensor imaging of the brain. Neurotherapeutics 4, 316–329. http://dx.doi.org/10.1016/j.nurt.2007.05.011.

Beaulieu, C., 2002. The basis of anisotropic water diffusion in the nervous system - a technical review. NMR Biomed. 15, 435–455. http://dx.doi.org/10.1002/nbm.782.

Benjamini, Y., Hochberg, Y., 1995. Controlling the false discovery rate: a practical and powerful approach to multiple testing. J. R. Stat. Soc. B. http://dx.doi.org/10.2307/2346101.

Boccard, S.G.J., Pereira, E.A.C., Moir, L., Aziz, T.Z., Green, A.L., 2013. Long-term outcomes of deep brain stimulation for neuropathic pain. Neurosurgery 72, 221–230. http://dx.doi.org/10.1227/NEU.0b013e31827b97d6. (discussion 231).

Brennan, F.H., Cowin, G.J., Kurniawan, N.D., Ruitenberg, M.J., 2013. Longitudinal assessment of white matter pathology in the injured mouse spinal cord through ultra-high field (16.4T) in vivo diffusion tensor imaging. NeuroImage 82, 574–585. http://dx.doi.org/10.1016/j.neuroimage.2013.06.019.

Chen, D.Q., DeSouza, D.D., Hayes, D.J., Davis, K.D., O'Connor, P., Hodaie, M., 2015. Diffusivity signatures characterize trigeminal neuralgia associated with multiple sclerosis. Mult. Scler. 1–13. http://dx.doi.org/10.1177/1352458515579440.

Desouza, D.D., Moayedi, M., Chen, D.Q., Davis, K.D., Hodaie, M., 2013. Sensorimotor and pain modulation brain abnormalities in trigeminal neuralgia: a paroxysmal, sensory-triggered neuropathic pain. PLoS One 8, e66340. http://dx.doi.org/10.1371/journal.pone.0066340.

DeSouza, D.D., Hodaie, M., Davis, K.D., 2014. Abnormal trigeminal nerve microstructure and brain white matter in idiopathic trigeminal neuralgia. Pain 155, 37–44. http://dx.doi.org/10.1016/j.pain.2013.08.029.

DeSouza, D.D., Davis, K.D., Hodaie, M., 2015. Reversal of insular and microstructural nerve abnormalities following effective surgical treatment for trigeminal neuralgia. Pain 156, 1112–1123. http://dx.doi.org/10.1097/j.pain.0000000000000156.

Dhople, A.A., Adams, J.R., Maggio, W.W., Naqvi, S.A., Regine, W.F., Kwok, Y., 2009. Long-term outcomes of Gamma Knife radiosurgery for classic trigeminal neuralgia: implications of treatment and critical review of the literature. Clinical article. J. Neurosurg. 111, 351–358. http://dx.doi.org/10.3171/2009.2.JNS08977.

Eller, J.L., Raslan, A.M., Burchiel, K.J., 2005. Trigeminal neuralgia: definition and classification. Neurosurg. Focus. 18, E3.

Fedorov, A., Beichel, R., Kalpathy-Cramer, J., Finet, J., Fillion-Robin, J.-C., Pujol, S.,

Bauer, C., Jennings, D., Fennessy, F., Sonka, M., Buatti, J., Aylward, S., Miller, J.V., Pieper, S., Kikinis, R., 2012. 3D Slicer as an image computing platform for the Quantitative Imaging Network. Magn. Reson. Imaging 30, 1323–1341. http://dx.doi.org/10.1016/j.mri.2012.05.001.

Herweh, C., Kress, B., Rasche, D., Tronnier, V., Troger, J., Sartor, K., Stippich, C., 2007. Loss of anisotropy in trigeminal neuralgia revealed by diffusion tensor imaging. Neurology 68, 776–778. http://dx.doi.org/10.1212/01.wnl.0000256340.16766.1d.

Hodaie, M., Coello, A.F., 2013. Advances in the management of trigeminal neuralgia. J. Neurosurg. Sci. 57, 13–21.

Jannetta, P.J., 1967. Arterial compression of the trigeminal nerve at the pons in patients with trigeminal neuralgia. J. Neurosurg. 26, 159–162. http://dx.doi.org/10.3171/jns.1967.26.1part2.0159.

Kondziolka, D., Lunsford, L.D., Flickinger, J.C., Young, R.F., Vermeulen, S., Duma, C.M., Jacques, D.B., Rand, R.W., Regis, J., Peragut, J.C., Manera, L., Epstein, M.H., Lindquist, C., 1996. Stereotactic radiosurgery for trigeminal neuralgia: a multi-institutional study using the gamma unit. J. Neurosurg. 84, 940–945. http://dx.doi.org/10.3171/jns.1996.84.6.0940.

Koopman, J.S.H.A., Dieleman, J.P., Huygen, F.J., de Mos, M., Martin, C.G.M., Sturkenboom, M.C.J.M., 2009. Incidence of facial pain in the general population. Pain 147, 122–127. http://dx.doi.org/10.1016/j.pain.2009.08.023.

Leal, P.R.L., Roch, J.A., Hermier, M., Souza, M.A.N., Cristino-Filho, G., Sindou, M., 2011. Structural abnormalities of the trigeminal root revealed by diffusion tensor imaging in patients with trigeminal neuralgia caused by neurovascular compression: a prospective, double-blind, controlled study. Pain 152, 2357–2364. http://dx.doi.org/10.1016/j.pain.2011.06.029.

Love, S., Coakham, H.B., 2001. Trigeminal neuralgia: pathology and pathogenesis. Brain 124, 2347–2360. http://dx.doi.org/10.1093/brain/124.12.2347.

Maarbjerg, S., Wolfram, F., Gozalov, A., Olesen, J., Bendtsen, L., 2015. Significance of neurovascular contact in classical trigeminal neuralgia. Brain 138, 1–9. http://dx.doi.org/10.1093/brain/awu349.

Moayedi, M., Weissman-Fogel, I., Salomons, T.V., Crawley, A.P., Goldberg, M.B., Freeman, B.V., Tenenbaum, H.C., Davis, K.D., 2012. White matter brain and trigeminal nerve abnormalities in temporomandibular disorder. Pain 153, 1467–1477. http://dx.doi.org/10.1016/j.pain.2012.04.003.

Mukherjee, P., Berman, J.I., Chung, S.W., Hess, C.P., Henry, R.G., 2008. Diffusion tensor MR imaging and fiber tractography: theoretic underpinnings. Am. J. Neuroradiol. 29, 632–641. http://dx.doi.org/10.3174/ajnr.A1051.

Nurmikko, T.J., Eldridge, P.R., 2001. Trigeminal neuralgia—pathophysiology, diagnosis and current treatment. Br. J. Anaesth. 87, 117–132. http://dx.doi.org/10.1093/bja/87.1.117.

Oesman, C., Mooij, J.J.A., Sc, M., Mooij, J.J.A., Ph, D., 2011. Long-term follow-up of microvascular decompression for trigeminal neuralgia. Skull Base 1, 313–321. http://dx.doi.org/10.1055/s-0031-1284213.ISSN.

Qazi, A.a., Radmanesh, A., O'Donnell, L., Kindlmann, G., Peled, S., Whalen, S., Westin, C.-F., Golby, A.J., 2009. Resolving crossings in the corticospinal tract by two-tensor streamline tractography: method and clinical assessment using fMRI. NeuroImage 47, T98–T106. http://dx.doi.org/10.1016/j.neuroimage.2008.06.034.

Ross, I., Robert, G., Ihaka, R., Gentleman, R., 1996. R: a language for data analysis and graphics. J. Comput. Graph. Stat. http://dx.doi.org/10.1080/10618600.1996.10474713.

Smith, S.M., Jenkinson, M., Woolrich, M.W., Beckmann, C.F., Behrens, T.E.J., Johansen-Berg, H., Bannister, P.R., De Luca, M., Drobnjak, I., Flitney, D.E., Niazy, R.K., Saunders, J., Vickers, J., Zhang, Y., De Stefano, N., Brady, J.M., Matthews, P.M., 2004. Advances in functional and structural MR image analysis and implementation as FSL. NeuroImage 23 (Suppl. 1), S208–S219. http://dx.doi.org/10.1016/j.neuroimage.2004.07.051.

Song, S.-K., Sun, S.-W., Ramsbottom, M.J., Chang, C., Russell, J., Cross, A.H., 2002. Dysmyelination revealed through MRI as increased radial (but unchanged axial) diffusion of water. NeuroImage 17, 1429–1436.

Song, S.K., Sun, S.W., Ju, W.K., Lin, S.J., Cross, A.H., Neufeld, A.H., 2003. Diffusion tensor imaging detects and differentiates axon and myelin degeneration in mouse optic nerve after retinal ischemia. NeuroImage 20, 1714–1722. http://dx.doi.org/10.1016/j.neuroimage.2003.07.005.

Song, S.K., Yoshino, J., Le, T.Q., Lin, S.J., Sun, S.W., Cross, A.H., Armstrong, R.C., 2005. Demyelination increases radial diffusivity in corpus callosum of mouse brain. NeuroImage 26, 132–140. http://dx.doi.org/10.1016/j.neuroimage.2005.01.028.